Experimental Eye Research 249 (2024) 110146

Contents lists available at ScienceDirect

Experimental Eye Research

journal homepage: www.elsevier.com/locate/yexer

Research article

Optical and retinal changes influenced by different lighting conditions

Elvira Orduna-Hospital [a,b,*], Juan J. Sanchez-Bautista [a], Guisela Fernández-Espinosa [a,b], María Arcas-Carbonell [a,b], Ana Sanchez-Cano [a,b]

[a] Departamento de Física Aplicada, Universidad de Zaragoza, 50009, Zaragoza, Spain
[b] Aragon Institute for Health Research (IIS Aragon), 50009, Zaragoza, Spain

ARTICLE INFO

Keywords:
Lighting conditions
Retinal curvature
Ocular aberrometry
Optical coherence tomography
Illumination

ABSTRACT

Retinal morphology, specifically in its curvature, and ocular aberrations change when the eye adapts to different lighting conditions, including photopic, scotopic, mesopic, blue light, and red light. Sixty healthy young subjects with refractive error less than ±4.00 D of sphere and 3.00 D of cylinder, not suffering from accommodative problems, ocular or systemic pathology, and not having used electronic devices half an hour before or having taken substances that alter the retina during the 2 h prior to the study were included. The subjects adapted to five lighting conditions, each for 5 min, in a controlled environment. Ocular aberrometry and Optical Coherence Tomography (OCT) were taken to capture images of the central and peripheral retina before (baseline measurements) and after adaptation to each lighting condition. The OCT images were exported and processed to analyze retinal curvature, obtaining parameters such as eccentricity, asphericity and shape factor. The results showed that the shape of the retina was hyperbolic prolate, becoming flatter in scotopic and blue light conditions, and more curved in mesopic conditions. Retinal curvature was closest to baseline under red light and photopic conditions. Aberrometric differences, particularly in the C(2,0) polynomial for defocus, showed higher values in mesopic, baseline, and scotopic conditions, and lower values in photopic, blue light, and red light. Significant differences were also observed in spherical aberrations C(4,0) and C(6,0), vertical coma C(3,-1), and trefoil C(3,-3). The spherical equivalent indicated more myopic values in mesopic, baseline, and scotopic conditions, and more hyperopic values in blue, photopic, and red light, suggesting a link between myopia and lower luminosity. This study concludes that illumination affects retinal curvature and ocular refraction, influencing myopia.

1. Introduction

Lighting changes are prevalent in our society and hold significant importance for daily activities and the physiology of living organisms. Among the various factors where lighting plays a crucial role, one of the most important is the circadian rhythm. This biological cycle, approximately 24 h in duration, regulates various physiological and behavioural functions in living beings, including humans. The circadian rhythm is primarily influenced by environmental cues, such as light and darkness, and is controlled by an internal "biological clock" located in the suprachiasmatic nucleus (SCN) of the hypothalamus in the brain (Monk et al., 1983; Van Dongen and Dinges, 2000). The circadian rhythm affects a wide variety of bodily processes, such as the sleep-wake cycle, determining periods of sleepiness and alertness; hormonal secretion, influencing the release of hormones such as cortisol and melatonin; body temperature, regulating the daily variation of body temperature; digestive function, modulating the processes of digestion and metabolism; and cognitive performance, impacting attention span, memory and other cognitive functions. Maintaining a regular circadian rhythm is crucial for health and well-being. Disturbances in this rhythm, such as those caused by night work, jet lag, or exposure to artificial light at night, can lead to sleep disorders and other health problems (Kofuji et al., 2016; Monk et al., 1983).

The intrinsically photosensitive ganglion cells (ipRGCs) are a type of retinal cells that detect light directly thanks to a photopigment called melanopsin, being especially sensitive to blue light. These cells are crucial for non-visual functions such as circadian rhythm regulation, as they transmit information about light to the SCN, synchronizing circadian rhythms with the light-dark cycle (Kofuji et al., 2016; Wirz-Justice et al., 2021). They also regulate the pupillary reflex, adjusting the size of

* Corresponding author. Departamento de Física Aplicada, Universidad de Zaragoza, 50009, Zaragoza, Spain.
E-mail addresses: eordunahospital@unizar.es (E. Orduna-Hospital), 797023@unizar.es (J.J. Sanchez-Bautista), guisela.fernandez3@gmail.com (G. Fernández-Espinosa), marcas@unizar.es (M. Arcas-Carbonell), anaisa@unizar.es (A. Sanchez-Cano).

https://doi.org/10.1016/j.exer.2024.110146
Received 18 July 2024; Received in revised form 17 October 2024; Accepted 1 November 2024
Available online 2 November 2024

the pupil in response to light, and the secretion of melatonin. So, the ipRGCs are essential for the body's adaptation to changes in environmental lighting and for maintaining circadian health, which significantly influences ocular responses, affecting organismal behaviours (Kofuji et al., 2016; Sergeeva et al., 2023).

For years, the refractive changes that occur in the eye in low light conditions have been investigated, revealing the appearance of a myopic refractive error (CHIN and HORN, 1956). Some time ago it was already observed that in scotopic conditions, when the pupil was in mydriasis, the spherical aberration of the eye increases from 0.75D to 1.75D, because the marginal rays focus before the retina. Apart from possible geometric aberrations, chromatic aberrations occur due to the difference in wavelength of light (Zhang and Zhu, 2022).

Nowadays, in vivo images of the retina and choroid can be obtained using optical coherence tomography (OCT), which uses low-coherence interferometry to produce axial images, allowing for the reconstruction of two-dimensional tomographic images of ocular structures (Lindenmaier et al., 2013). Thus, it has been seen that choroidal thickness varies depending on the lighting conditions to which the eyeball is subjected, possibly due to the change in the activity of the cones and rods, together with the post-illumination pupillary response mediated by cells ipRGC (Lou and Ostrin, 2020). Additionally, variations in retinal curvature can be observed and measured by selecting the retinal pigment epithelium (RPE) as a reference point from these images. Due to its high melanin content, the RPE absorbs less infrared light, resulting in greater reflectivity facilitating its identification and precise delineation (Spaide and Curcio, 2011). Another technique that provides information about the shape of the eyeball in three dimensions is the Magnetic Resonance Imaging (MRI), which allows to know the shape of the eyeball (Beenakker et al., 2015). Furthermore, the shape and curvature of the retina and choroidal thickness, correlated with ocular axial length (AL), are also related to the development of myopia (Liu et al., 2018; Orduna-Hospital et al., 2023; Zhu et al., 2023), which makes it important to study environmental lighting as an influential parameter in its development.

The shape of the retina is important for understanding myopia development. Various custom-built or modified instruments measure peripheral eye length, especially with increased research on myopia onset and progression (Koumbo Mekountchou et al., 2020).

Cheng et al. (1992) observed in a small cohort that all eyes shared the same sphero-elliptical shape, regardless of ametropia. Another analysis (Atchison et al., 2004) described myopic eyes as elongated but found that approximately equal proportions of myopic eyes fit both global expansion and axial elongation models. Additionally, eye models based on retinal contours fitting a general ellipsoid, incorporating both decentration and orientation, indicated that the retinal shapes of myopic eyes deviate more from an ellipsoid than those of emmetropic eyes (Li and Fang, 2021). This study found that both myopic and emmetropic eye models have oblate retinas, with the oblateness being less pronounced in myopes, a pattern supported by other data (Atchison et al., 2005; Pope et al., 2017; Verkicharla et al., 2016, 2017).

The hypothesis of this study proposes that different ambient lighting conditions can modify retinal curvature and cause significant optical changes in ocular aberrations, suggesting dynamic eye adaptation to varying luminosity levels and light spectra. The primary purpose is to observe changes in retinal morphology, specifically curvature, and ocular aberrations when the eye adapts to different lighting conditions (photopic, scotopic, mesopic, blue light, and red light).

2. Material and methods

2.1. Sample description

The study was conducted following the approval of the Clinical Research Ethics Committee of Aragón (CEICA), reference number PI21-074, and adhered to the principles established in the Declaration of Helsinki. A sample of 60 healthy subjects, 40 women and 20 men, was selected, with measurements taken only from the right eye (OD), resulting in a total of 60 eyes under each lighting condition. Participants were informed in advance about the tests to be conducted and signed a consent form indicating their agreement to participate in the study and data collection. The necessary devices for the tests were in the laboratory of the Department of Applied Physics at the University of Zaragoza, and the measurements were conducted always by the same experimented examiner. All participants were adults, aged between 20 and 34 years, and healthy, with refractive errors less than ±4.00 D sphere and 3.00 D cylinder. The exclusion criteria for participation in the study were suffering from accommodative or binocular dysfunctions, amblyopia, or strabismus; having a decimal visual acuity (VA) less than 0.8 in either eye; suffering from any ophthalmic or systemic pathology affecting vision; having ocular media opacification; using electronic devices half an hour before the study measurements or consuming substances that could alter the retina, such as alcohol, coffee, or tobacco, 2 h before the experiment. To adapt to the different lighting conditions, participants were asked to remove their optical lenses to avoid any potential filtering of light wavelengths, ensuring the most reliable results possible.

2.2. Used devices

For ocular adaptation to the different lighting conditions, a controlled lighting box (Fig. 1) located in the laboratory under scotopic environmental conditions was used. It was a lighting grey box, Munsell N7, which was made up of three vertical walls, a ceiling and a base, and two LED luminaires linked to an 8th generation iPad model A2270 (Apple Inc, Cupertino, California, USA), that allowed the five lighting conditions to be configured for study. These luminaires were equipped with three LEDs: a cool white LED, a blue LED with a peak emission wavelength at 464 nm and a full width at half maximum (FWHM) of 24 nm, and a red LED with a peak emission wavelength at 631 nm and a FWHM of 18 nm. The values of the different lighting conditions were measured with the StellarNet Black-Comet spectroradiometer (StellarNet Inc., Tampa, Florida), thus ensuring consistency in the measurement conditions in all participants.

2.3. Aberrometer

The IRX3 Shack-Hartmann clinical aberrometer (Imagine Eyes, Orsay, France) used for this study consists of an infrared light source with a wavelength of approximately 780 nm. This equipment is a Hartman-Shack type aberrometer where light enters the pupil, reaches the retina and is reflected, allowing the receiving system to analyze the directional information of the wave front after correct alignment with the eye. Subsequently, the system calculates the wavefront aberrations by comparing it with an ideal wavefront, allowing the values of the different Zernike polynomials to be obtained.

Six aberrometric measurements were conducted per eye. The first served as a baseline measurement. Subjects then adapted to one of five lighting conditions (photopic, mesopic, scotopic, blue light, or red light) for 5 min in the lighting box, with conditions randomly selected to prevent bias, followed by a 15-min rest period where participants refrained from using any screens or devices. After adaptation, an immediate aberrometric measurement was taken. The time span for measurements per individual was approximately 1 h and 45 min because all lighting conditions were tested in a single session to maintain consistency in the experimental environment. To obtain comparable intra-subject values across different lighting conditions, all aberrometric data for the ODs, with a 4 mm pupil diameter, were exported and classified by lighting condition in an Excel database (Microsoft® Office Excel 365, Microsoft Corporation, Redmond, WA, USA), including up to the 6th order of Zernike polynomials.

To visualize the average aberrations under each lighting condition,

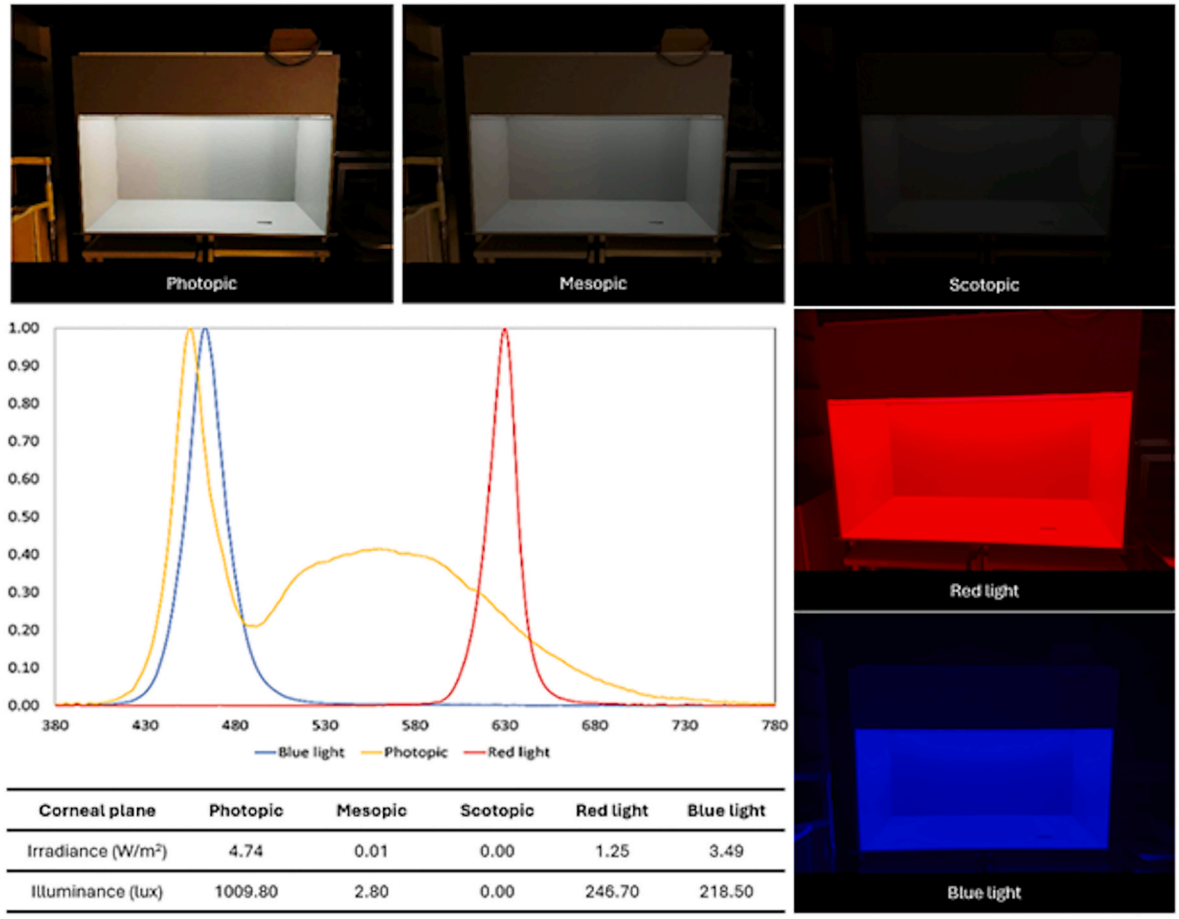

Corneal plane	Photopic	Mesopic	Scotopic	Red light	Blue light
Irradiance (W/m²)	4.74	0.01	0.00	1.25	3.49
Illuminance (lux)	1009.80	2.80	0.00	246.70	218.50

Fig. 1. Image of the controlled lighting cabin where the subjects were adapted to each of the five lighting conditions. Normalized spectral irradiance (W/m^2) of the light that reaches the corneal plane with each illumination. Blue light peaks at 464 nm and red light at 631 nm; mesopic lighting conditions was obtained, dimming the photopic spectra. (For interpretation of the references to colour in this figure legend, the reader is referred to the Web version of this article.)

we used custom code in MatLab R2022a (MathWorks Inc., 2022) to create colour maps and evaluate optical quality parameters such as the Point Spread Function (PSF), including simulations of uncorrected vision. Aberrometer data were processed in Matlab, yielding refractive error and PSF information for each lighting condition. This method allowed for the isolation of specific aberrations by setting the value of each Zernike coefficient to 0, except for the polynomials under evaluation.

2.4. Optical coherence tomography (OCT)

The OCT device used for retinal imaging in this study was the 3D OCT-1000 (Topcon Corporation, Tokyo, Japan) using the macular cube protocol, which scans 128 consecutive horizontal cross-sections (B-scans) over a 6 × 6 mm area, with two measurements per eye. The first measurement centered on the fovea, covering the central 30° of the retina and generating 128 images 6 mm in length. The second measurement involved shifting the fixation stimulus 15° temporally, obtaining images of the peripheral temporal retina. This process was conducted at baseline and repeated after 5 min of adaptation to each lighting condition (scotopic, photopic, mesopic, blue light, and red light), resulting in 12 measurements per eye. Low-quality scans were discarded and repeated. Due to time constraints and the risk of the retina reverting to its baseline state, we prioritized a single, rapid measurement by the most experienced investigator to capture the retinal state accurately and reduce potential artifacts. Although we initially considered taking multiple measurements, research has demonstrated the reliability of single high-quality OCT images and the inter- and intra-observer repeatability and reproducibility of OCT measurements (Baumann et al., 1998; Sala-Puigdollers et al., 2018; Sanchez-Cano et al., 2014).

2.5. Retina data export protocol

To export central and peripheral retinal images obtained with the OCT, the TopcomExtract 1.0 program (University of Zaragoza, Zaragoza, Spain) was used. OCT files in *.FDA format were processed and converted into images. For each subject, 128 PNG images were extracted per *.FDA file, with the image showing the foveal reflection selected as the central cut, along with the two upper and two lower cuts, resulting in five central retinal sections per file. This process was repeated for 12 files per subject, covering both baseline and post-adaptation to each lighting condition. For analyzing the five images per measurement, the ImgOCT 1.12 program (University of Zaragoza, Zaragoza, Spain) was employed. Image 1 of 5 on the left, corresponding to the peripheral retina, and image 1 of 5 on the right, corresponding to the central retina, were selected for analysis.

As shown in Fig. 2A, four trapezoid-shaped points were selected to join the central retina with the temporal peripheral retina, providing the best results. These points included one in the center of the foveal depression, another at the intersection of the retinal nerve fiber layer (RNFL) with the fovea, another in the RPE, and a final one further in the RNFL. Points with the same number had to be positioned in the same area of the central retina (Fig. 2B). Using these points, the image was processed, and the program combined the retinal images into a single image (Fig. 2C). This process was repeated to combine the five peripheral images with the five central ones, resulting in five 9 mm long retinal

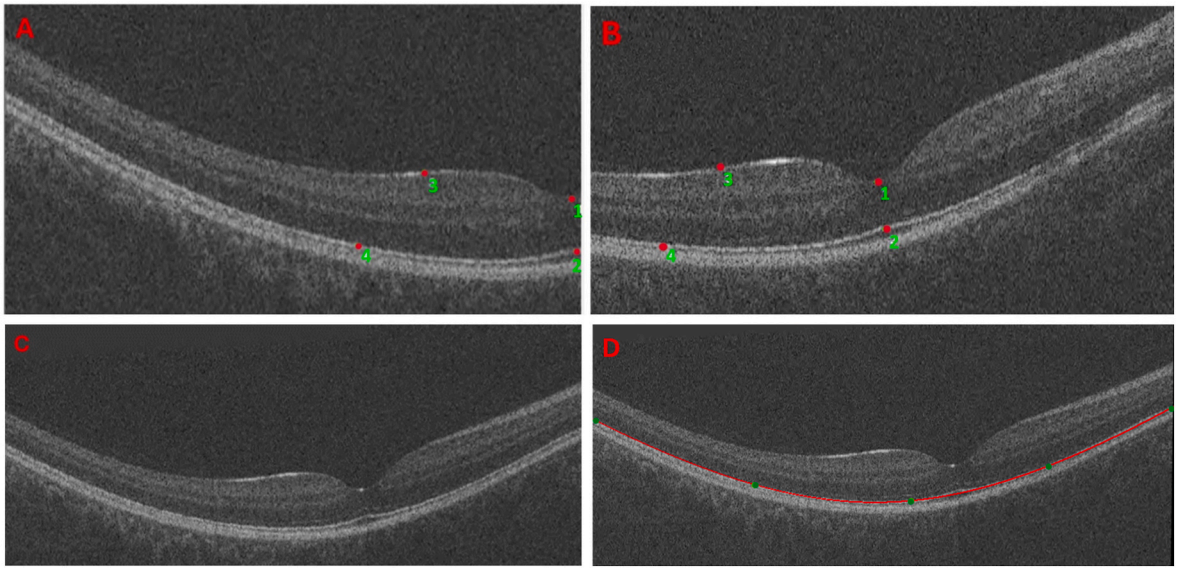

Fig. 2. **A:** The four red points marked on temporal peripheral retinal image. **B:** The four red points marked on the central retinal image. **C:** Image resulting from the unionof the peripheral and central images by the ImgOCT 1.12 program. **D:** Joined image, with the five green points selected for automatic creation of the curve (red line) and adjustment parameters to the conic: eccentricity (e), asphericity (Q) and the shape factor (p). (For interpretation of the references to colour in this figure legend, the reader is referred to the Web version of this article.)

slices. Each resulting image was processed in another section of the ImgOCT 1.12 program, where five points of the retinal profile corresponding to the RPE were selected. The program then calculated the conic adjustment (Fig. 2D), obtaining retinal curvature descriptor parameters such as eccentricity (e), asphericity (Q), and shape factor (SF). Data from the five cuts per measurement were automatically saved in a text file and recorded in an Excel database.

2.6. Calculation of eccentricity, asphericity and retinal shape factor

The calculation of the retinal curvature triple (e, Q, SF) was based on fitting the curve to the function of the general conic equation (Eq. (1)):

$$ax^2 + 2hxy + by^2 + 2gx + 2fy + n = 0 \quad \text{(Eq.1)}$$

Within the ImgOCT 1.12 program, the retinal curvature values of each image are governed by a series of coordinates that vary depending on the arrangement of each of the five points placed manually by the experienced observer. These coordinates are used to calculate the parameter e (Eq. (2)) and its sign (Eq. (3)):

$$e^2 = \frac{2\sqrt{(a-b)^2 + 4h^2}}{\sigma(a+b) + \sqrt{(a-b)^2 + 4h^2}} \quad \text{(Eq.2)}$$

$$\sigma = sign\left(nh^2 - abn + af^2 - 2hfg + bg^2\right) \quad \text{(Eq.3)}$$

The Q factor (Eq. (4)) describes the degree of deviation of the ellipse with respect to a circle, from the center to the periphery, if Q = 0, then e = 0 and a perfect circle is obtained. If the value of Q is negative (Q < 0) it will be a prolate surface, the curvature gradually increases towards the center. On the other hand, when Q is positive (Q > 0) it is an oblate surface, which is flatter in the center and more curved towards the periphery (Holladay and Janes, 2002).

$$Q = -e^2 \quad \text{(Eq.4)}$$

Finally, both parameters were correlated with the SF (Eq. (5)), which describes the geometry of the curve.

$$SF = 1 - Q \quad \text{(Eq. 5)}$$

From the results found after adjusting to the conic, a text file was created with the parameters of interest for all the ODs analyzed and for each type of lighting.

2.7. Statistical analysis

The data collected for the variables throughout the study were exported to Excel databases and subsequently processed using the Statistical Package for the Social Sciences (SPSS 24.0 inc., Chicago, IL, USA) for result analysis. Descriptive statistics of the sample were performed for the numerical variables, calculating the mean, standard deviation (SD), maximum, and minimum values of each. The Kolmogorov-Smirnov test determined that the variables did not follow a normal distribution, so non-parametric tests for multiple related samples (Friedman test) were applied. This was used to examine if there were differences in the variables of retinal morphology (e, Q, and SF) and aberrometric variables, comparing the six lighting conditions with each other. Bonferroni correction was applied for fifteen possible combinations, so a p-value <0.0003 was considered statistically significant. Subsequently, the variables under different lighting conditions were compared pairwise (scotopic vs. photopic conditions, etc.), using non-parametric tests for two related samples, applying the Wilcoxon signed-rank test and considering a p-value <0.05 as statistically significant.

3. Results

The sample consisted of 60 participants, with an average age of 23.57 ± 3.45 years (range: 20–34 years). Only the OD was included, with an average spherical equivalent (M) of −1.31 ± 1.83 D. The sample comprised 20 men and 40 women.

3.1. Retinal changes

When studying retinal curvature under different lighting conditions, the average values of the conic parameters (e, Q, SF) were very similar (Fig. 3A). The greatest differences from baseline (e = 1.5007, Q = −2.5841, SF = 3.5805) were observed in mesopic conditions (e = 1.4584, Q = −2.4750, SF = 3.4913), which were lower, and in scotopic (e = 1.5499, Q = −2.7339, SF = 3.7339) and blue light conditions (e =

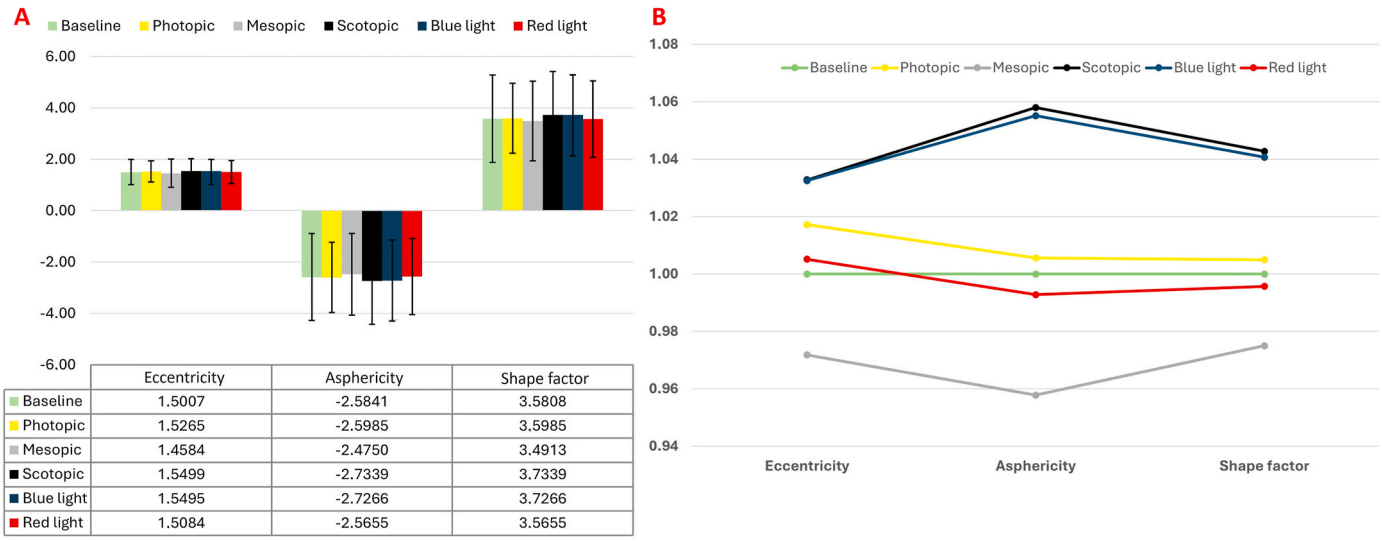

	Eccentricity	Asphericity	Shape factor
Baseline	1.5007	-2.5841	3.5808
Photopic	1.5265	-2.5985	3.5985
Mesopic	1.4584	-2.4750	3.4913
Scotopic	1.5499	-2.7339	3.7339
Blue light	1.5495	-2.7266	3.7266
Red light	1.5084	-2.5655	3.5655

Fig. 3. A: Mean results ± standard deviation (represented with error bars) of the retinal curvature parameters (eccentricity, asphericity and shape factor) of the baseline measurement and the different lighting conditions (photopic, mesopic, scotopic, blue light and red light). **B:** Representation of the relative mean values of retinal eccentricity, asphericity and shape factor with the five lighting conditions with respect to the baseline measurement to which a value of 1.00 is assigned in the three parameters. Friedman test with Bonferroni correction ($p < 0.0003$) showed no statistically significant differences across the six lighting conditions. (For interpretation of the references to colour in this figure legend, the reader is referred to the Web version of this article.)

1.5495, Q = −2.7266, SF = 3.7266), which were higher. The values closest to baseline were found under red light (e = 1.5084, Q = −2.5655, SF = 3.5655) and photopic conditions (e = 1.5265, Q = −2.5985, SF = 3.5985). Since the eccentricity values exceed unity, the predominant retinal shape in this study was hyperbolic, and the negative asphericity values indicate it was prolate (Fig. 3A).

Relative values of e, Q, and retinal SF were calculated relative to baseline measurements (Fig. 3B). Scotopic and blue illumination conditions exhibited similar behaviors, with relative values of the three parameters higher than those in baseline, suggesting a flatter retina in both cases. Conversely, red and photopic conditions showed behaviors like baseline values. Mesopic lighting conditions exhibited lower values of e, Q, and SF, indicating greater retinal curvature.

When comparing retinal eccentricities across different lighting conditions, significant differences were observed only between mesopic and scotopic light ($p = 0.041$), with scotopic light showing the flattest eccentricity. Comparisons between other lighting conditions did not yield significant differences (Table 1A). However, a relatively low p-value was found when comparing blue light with mesopic light ($p = 0.137$), indicating non-significant but noticeable variations, with the retina appearing more curved in mesopic conditions and flatter in blue light (Table 1B).

Table 1
A. Statistical significance, indicating the p-value, when comparing the retinal eccentricity in scotopic lighting conditions with the retinal eccentricity that occurs with the rest of the lighting conditions. **B.** Statistical significance, indicating the p-value when comparing the retinal eccentricity in blue lighting conditions with the retinal eccentricity that occurs with the rest of the lighting conditions. Statistically significant differences ($p < 0.05$), calculated with the Wilcoxon signed-rank test for two related samples, are marked in bold.

A. Scotopic retinal eccentricity vs. other illuminations

Scotopic vs.	Baseline	Photopic	Mesopic	Blue light	Red light
p-value	0.291	0.475	**0.041**	0.922	0.566

B. Retinal eccentricity with blue illumination vs. other illumination

Blue light vs.	Baseline	Photopic	Mesopic	Scotopic	Red light
p-value	0.423	0.250	0.137	0.922	0.556

3.2. Aberrometric changes

The analysis of Zernike coefficients following each aberrometric measurement revealed differences in low-order aberrations (LOA). Specifically, the defocus term C(2,0) indicated myopization, with higher values observed in mesopic (0.762 μm), baseline (0.729 μm), and scotopic conditions (0.672 μm), and lower values under blue light (0.657 μm) and red light (0.576 μm) (Fig. 4). Variations in the oblique astigmatism term C(2,-2) ranged from −0.003 μm under red and blue light to 0.021 μm under baseline conditions. Horizontal astigmatism C(2,2) showed variations ranging from −0.152 μm under mesopic conditions to −0.101 μm under red light (Fig. 4).

However, it should be noted that despite the high variability indicated by the standard deviation values relative to the average described, statistically significant differences were observed only in certain cases. Specifically, significant differences were found when comparing the defocus term C(2,0) between scotopic and red light conditions ($p = 0.031$), and near the significance threshold in scotopic versus blue light conditions ($p = 0.072$).

In the study of the high order aberrations (HOA) coefficients, certain differences were found, especially in the trefoil C(3,-3) and vertical coma C(3,-1), and in the primary spherical aberration C(4,0) and secondary C(6.0). (Fig. 5). Specifically, in the primary spherical aberration C(4.0), there were significant differences in the scotopic-mesopic ($p = 0.016$), scotopic-red ($p = 0.019$) and scotopic-blue ($p = 0.028$) analysis (Fig. 5A).

Similarly, significant differences were observed in secondary spherical aberration C(6,0) between scotopic and mesopic ($p = 0.031$), scotopic and red ($p = 0.043$), scotopic and blue ($p = 0.017$), and scotopic and photopic ($p = 0.009$) conditions. Additionally, statistically significant differences were found between baseline and photopic conditions ($p = 0.007$), and near the threshold of significance between scotopic and red conditions ($p = 0.069$) (Fig. 5B).

To aid in result interpretation, the M in D was calculated from the Zernike coefficients measured (Eq. (6)) for each different lighting conditions for a pupil diameter of R = 4 mm (Fig. 6):

$$M = \left(4^{*\ 3\ *C(2,0)-12*\ \ 5*\ C(4,0)+24*\ \frac{7\ *C(6,0)}{\left(\frac{R}{2}\right)^6}}\sqrt{}\right) \quad \text{(Eq. 6)}$$

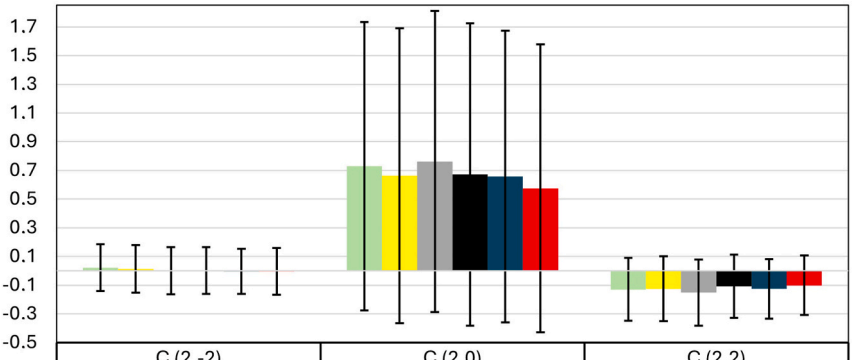

	C (2,-2)	C (2,0)	C (2,2)
Baseline	0.021	0.729	-0.130
Photopic	0.014	0.663	-0.124
Mesopic	0.000	0.762	-0.152
Scotopic	0.002	0.672	-0.108
Blue light	-0.003	0.657	-0.126
Red light	-0.003	0.576	-0.101

Fig. 4. Mean Zernike coefficients in μm ± standard deviation (represented with error bars) of second-order aberrations: oblique astigmatism C(2,-2), defocus C(2,0) and horizontal astigmatism C(2,2), for the six lighting conditions.

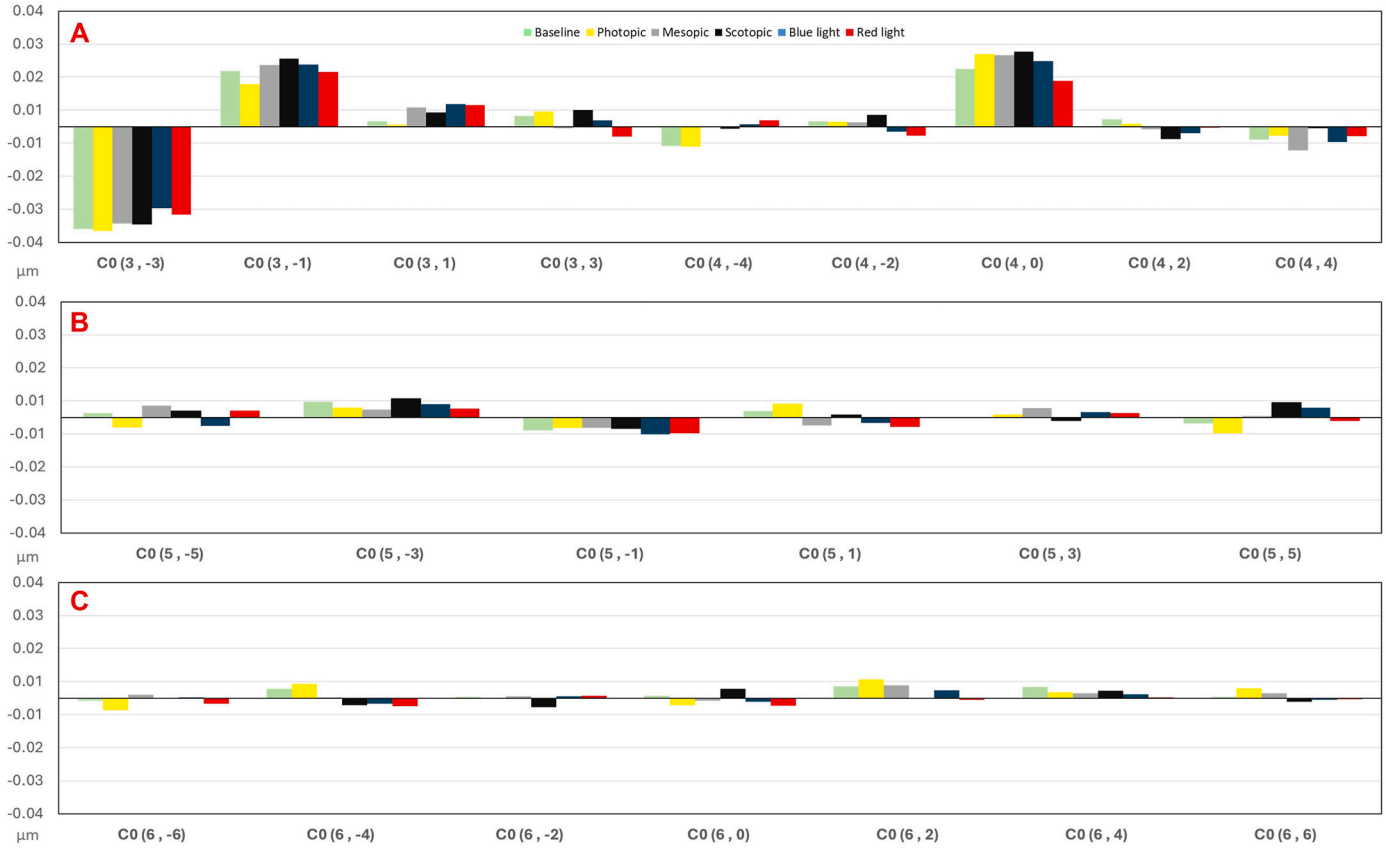

Fig. 5. Bar graph of mean Zernike coefficients in μm representing higher-order aberrations for the six measured lighting conditions. **A:** Third and fourth order. **B:** Fifth order **C:** Sixth order.

Regarding the baseline M value (−1.158 D), minimal variation in M was observed in mesopic (−1.162 D) and scotopic conditions (−1.057 D), indicating little change after adaptation to reduced light levels and complete darkness, respectively. Photopic, blue light, and red-light conditions showed more positive M values compared to baseline: −0.951 D, −0.987 D, and −0.876 D, respectively, indicating a less myopic outcome than baseline while still maintaining myopization in all cases.

Variations in wavefront aberrations affected the quality of retinal images, as observed in qualitatively analyzed PSFs under different lighting conditions. While differences were subtle, changes in shape and size were evident across the PSF maps. Blur was a significant factor due

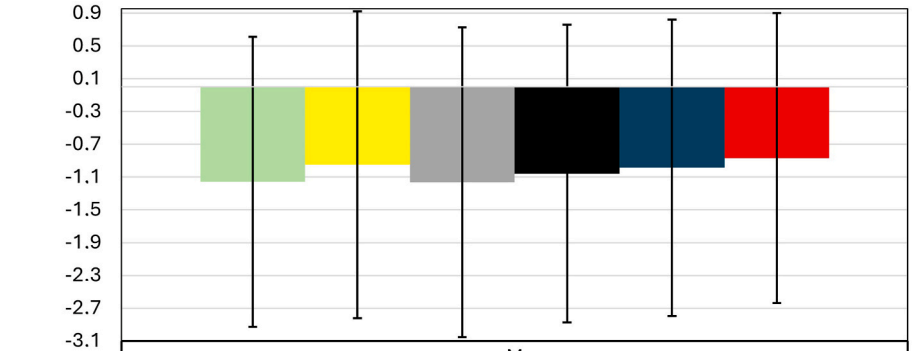

	M
Baseline	-1.158
Photopic	-0.951
Mesopic	-1.162
Scotopic	-1.057
Blue light	-0.987
Red light	-0.867

Fig. 6. Mean spherical equivalents (M) in D ± standard deviation (represented with error bars) for each of the six lighting conditions measured.

to participants not being previously corrected, with LOAs contributing significantly (Fig. 7A). Nonetheless, the patterns observed were generally similar across conditions, suggesting that variations in refractive error did not lead to significant changes in aberrations.

PSFs in scotopic, baseline, and mesopic conditions exhibited similar oval-shaped images. Photopic conditions began to show shape variations, particularly in the upper part of the map, with noticeable differences emerging in monochromatic illuminations (blue and red), where sizes decreased. The PSF image under red light appeared more spherical and less oval compared to other conditions (Fig. 7A).

A comparable analysis of wavefront maps revealed significant similarity among them, predominantly showing a myopic pattern with horizontal astigmatism. While subtle differences were noticeable between images, notable changes in astigmatism were observed particularly in red light and scotopic conditions compared to the other four conditions. It is important to note that since subjects were uncorrected, these maps reflect the average aberrations of the sample selected (Fig. 7B).

Focusing solely on the spherical components C(2,0), C(4,0), and C (6,0) in the PSF, differences could be observed. Scotopic, mesopic, baseline, and photopic conditions exhibited a similar size distribution. However, under red and blue light illuminations, a more compact light distribution was evident, resulting in a smaller apparent PSF. Particularly notable was the PSF obtained under red light, which showed a distinctly smaller pattern (Fig. 8). The observed increase in the PSF size under blue light conditions, compared to red light, could be influenced by Longitudinal Chromatic Aberration (LCA), as blue light typically experiences a greater degree of defocus due to its shorter wavelength and focal shift relative to red light. This effect leads to a broader PSF in blue light adaptation, highlighting the influence of chromatic aberrations on ocular optics.

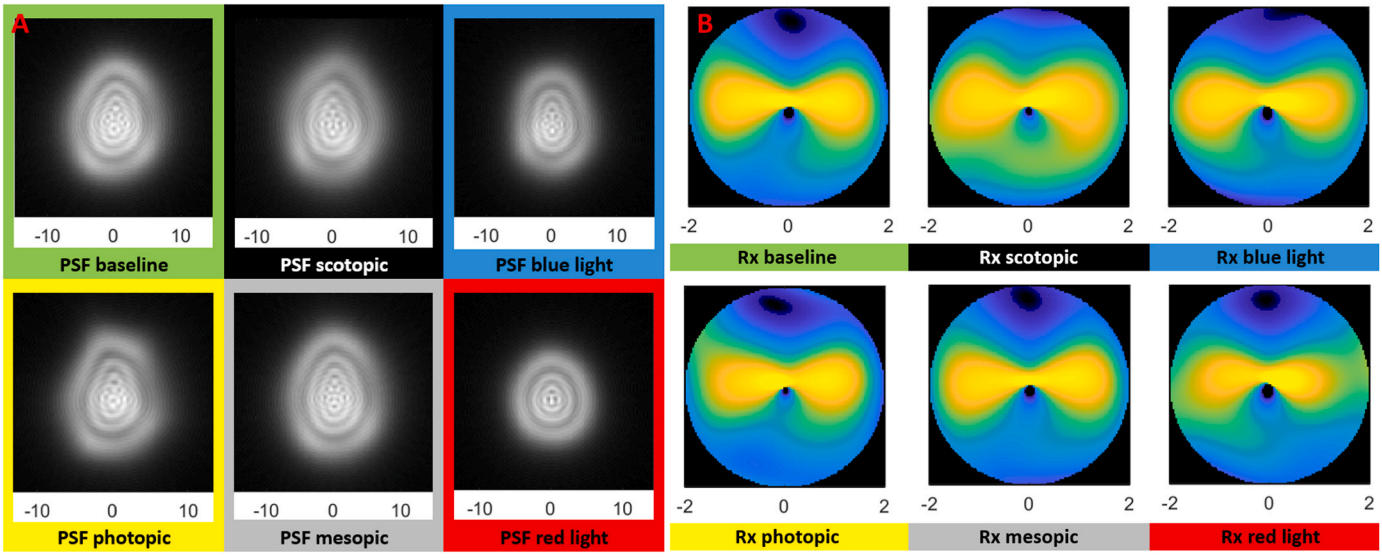

Fig. 7. A: Representation of the PSFs in the six lighting conditions on a scale of (−10, 10) μm (baseline, scotopic, blue light, photopic, mesopic and red light). **B:** Representation of the refractive wavefront (Rx) maps in the different lighting conditions (baseline, scotopic, blue light, photopic, mesopic and red light) taking into account all the Zernike coefficients. (For interpretation of the references to colour in this figure legend, the reader is referred to the Web version of this article.)

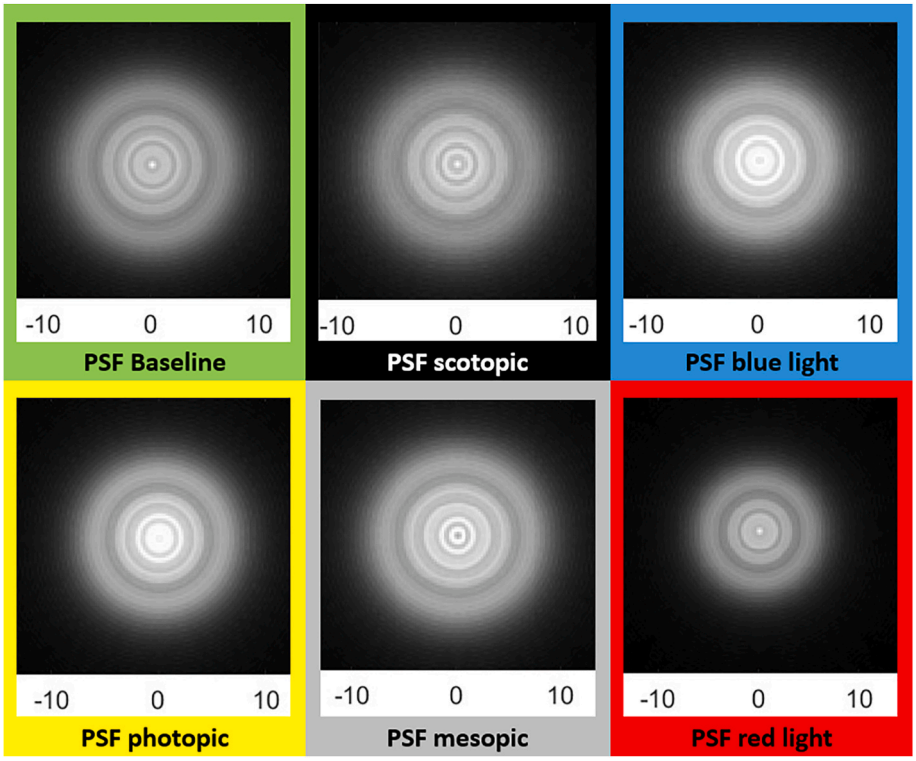

Fig. 8. Representation of the PSFs exclusively conditioned by spherical pattern aberrations: defocus C(2,0), primary spherical C(4,0) and secondary spherical C(6,0) in the different lighting conditions on a scale of (−10, 10) μm (baseline, scotopic, blue light, photopic, mesopic and red light).

4. Discussion

This study investigated variations in retinal curvature and aberrometric changes following 5-min exposures to different lighting conditions in a group of healthy young adults. Using OCT analysis and specialized software, triple values (e, Q, SF) were obtained from retinal images to assess parameter variations under each illumination type, referencing the RPE. Aberrometric values post-illumination were analyzed relative to baseline measurements, serving as a reference point for comparison.

The use of a 5-min adaptation period in this study was supported by our previous research (Orduna-Hospital et al., 2023) indicating that changes in retinal thickness and morphology could occur within brief exposure times to varying light conditions. Other authors (Cameron et al., 2020) observed the rapid adaptation of the human retina to light changes, with physiological responses visible in as little as 5 min. In our present findings, the 5-min duration effectively captured the dynamic shifts in retinal curvature under different lighting conditions, validating our methodological choice.

4.1. Retinal morphology

Our study observed variations in retinal morphology, indicating alterations in retinal curvature under different lighting conditions. While most changes were not statistically significant, except for the mesopic-scotopic comparison ($p = 0.041$) and an observable difference between mesopic-blue light ($p = 0.137$), these findings suggest retinal adaptation to environmental stimuli.

In our previous study (Orduna-Hospital et al., 2023) conducted under comparable conditions, changes in retinal curvature were also noted alongside alterations in retinal thickness after adaptation to varying illuminations. Specifically, we reported increased retinal thickness and greater retinal eccentricity in scotopic conditions, indicating greater flattening of the retina. We found higher eccentricity in the peripheral retina under scotopic conditions and lower eccentricity in red light and mesopic conditions, while in the central retina, eccentricity was higher in mesopic and photopic conditions and lower in red light. A significant distinction in the current study compared to our previous work (Orduna-Hospital et al., 2023) is the integration of both temporal and central retinal images into a single 9 mm image, while in the previous study, we analyzed the retina by dividing it into peripheral and central segments (6 mm each). In the present findings, scotopic conditions showed higher eccentricity (1.5499), indicating greater flattening, consistent with our earlier results. Photopic conditions showed lower eccentricity (1.5265), indicating greater curvature compared to scotopic conditions, while mesopic light exhibited even lower eccentricity (1.4584), suggesting increased curvature.

Comparison of monochromatic illuminations revealed that blue light induced greater retinal eccentricity (1.5495) compared to red light (1.5084), aligning with the findings of our previous study (Orduna-Hospital et al., 2023), where blue light similarly led to greater eccentricity in both central and peripheral retina. This suggests that red wavelengths induce greater retinal curvature, potentially influenced by the arrangement and quantity of red and blue cones in the retina (Cameron et al., 2020).

When merging retinal images of myopic subjects, better superimposition was observed, likely due to differences in peripheral retinal thickness compared to hyperopic or emmetropic individuals. Myopic subjects generally exhibit thinner retinas (Cheng et al., 2010), and may display greater curvature (Fig. 9), facilitating program adjustment. Flatter retinas could complicate conic adjustments in the program, particularly if points were inaccurately positioned. Other authors such as Lim et al. found that myopic eyes had less oblate posterior retinal shape and that Q decreased as age increased. They also found an increased AL and a decreased Q in myopia, being less oblate (Lim et al., 2020), finding that the curvature was flatter in the retinal periphery than in the fovea (Atchison and Smith, 2023).

MRI data from individuals aged 18–36 years (Atchison et al., 2005) demonstrated that the majority of myopic eyes exhibit oblate retinal configurations, rather than prolate, with significant inter-subject

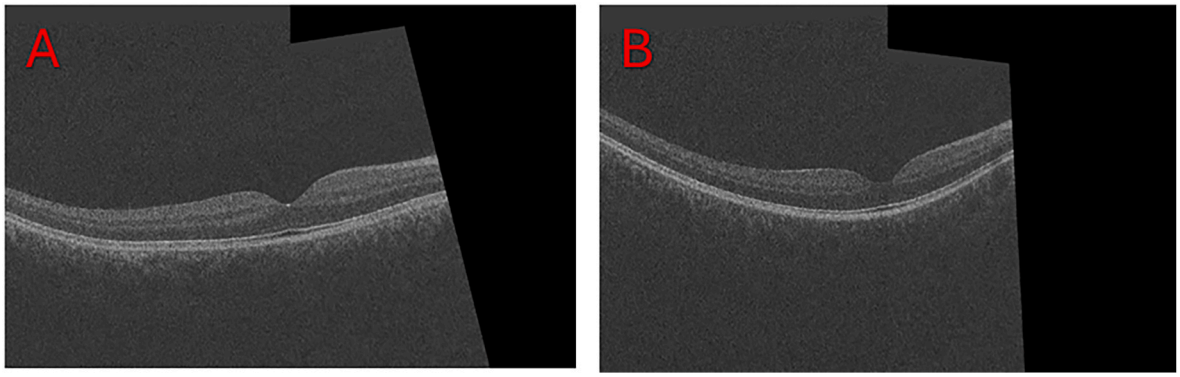

Fig. 9. **A:** Attached temporal and central retina of an emmetropic subject. **B:** Attached temporal and central retina of a myopic subject.

variability observed among individuals with analogous refractive errors. Emmetropic eyes predominantly displayed oblate shapes, characterized by an increase in curvature toward the equator. As the degree of myopia intensified, the retinal shape progressively became less oblate. Notably, only a minority of myopic eyes presented with a prolate form, characterized by a flattening towards the equator. Ishii et al. (2011) observed that in children, the progression of myopia involves a transition from an oblate to a prolate eyeball configuration, though the shapes of the eye and retina can differ. An eye may be classified as prolate when its AL surpasses its width or height, even if its retinal shape remains oblate. Simply categorizing eye shape as prolate or oblate is inadequate without a comprehensive understanding of the contributing factors; in myopia, a prolate configuration likely entails a steepening of the retina near the posterior pole and a flattening away from it (Verkicharla et al., 2012). Differences in retinal shape from nasal to temporal areas were noted with steeper retinas in older subjects (Faria-Ribeiro et al., 2014). MRI studies have indicated that a less oblate posterior ocular morphology, characterized by lower Q values, is correlated with myopic M and increased AL, typical features of myopic eyes. Non-myopic eyes exhibit more uniform expansion, whereas myopic eyes primarily elongate along the axial dimension, leading to a less oblate shape even in the early stages of myopia development. This study demonstrated a consistent association between myopic refraction, increased AL, and a more prolate ocular shape, suggesting that as myopic eyes age and myopia progresses, they tend to maintain a more prolate configuration, even if the AL decreases (Lim et al., 2020). Ethnic variations in this trend have also been observed (Mohd-Ali et al., 2022; Verkicharla et al., 2017).

Additionally, the retinal changes observed under varying lighting conditions may be influenced by physiological factors such as alterations in blood flow and metabolic activity. Light exposure can affect the retinal vasculature, leading to changes in blood flow, which may subsequently influence retinal thickness and morphology. Furthermore, the relationship between light stimuli and retinal responses can activate signalling pathways that regulate retinal function. For instance, studies have shown that illumination can modulate the expression of vascular endothelial growth factor (VEGF) and other factors involved in retinal blood flow regulation (Antemie et al., 2023; Chistyakov et al., 2020; Penn et al., 2008).

Quantitative analysis of retinal shape using OCT can be complicated by various optical distortions inherent to imaging the posterior segment. While our Fourier domain OCT systems provide adequate speed and sensitivity, they are susceptible to artifacts that can limit their axial range. In our study, it was essential to ensure the accuracy of the images to obtain a series of measurements for comparison with the baseline images. These limitations might be mitigated by using whole retina images, which seem comparable to MRI measurements (McNabb et al., 2019). Whole-eye imaging offers multiple applications by enabling the measurement of both the anterior and posterior segments of the eye using the same instrument. This approach facilitates an accurate determination of the true retinal shape (Frisken et al., 2023). Our images were used to compile the evaluated retinas, but artifacts could occur during peripheral measurements, like issues encountered when measuring refractive error and eye length with commercial devices (Atchison and Rozema, 2023).

4.2. Aberrations

Our baseline findings showed a more myopic tendency (−1.158 D) compared to expectations, which was consistent with the M values observed in mesopic (−1.162 D) and scotopic (−1.057 D) conditions. Typically, the baseline M value would be expected to align more closely with photopic conditions, given the experiment's timing and ambient conditions. This discrepancy may be attributed to the young age of the subjects and their robust accommodative abilities. Prior use of electronic devices or studying could potentially influence baseline measurements towards slight myopia, despite instructions to abstain from device use for at least half an hour before testing, which may have been insufficient.

Various studies show that in low light conditions, subjects tend to be more myopic, Wald and Griffin (WALD and GRIFFIN, 1947) talk about a study of 21 patients, where the average difference is about 0.59 D, in another study (Koomen et al., 1951) indicated variations of approximately 1.5–2.0 D. While other research suggested a myopic shift of around 0.80 D in similar conditions (Artal et al., 2012). However, factors like spherical aberration may also contribute to these results. Despite the theory of chromatic aberration due to the Purkinje effect, Wald and Griffin estimated its contribution to nocturnal myopia to be 0.3 D (WALD and GRIFFIN, 1947).

In our study, differences were observed between blue light and red light conditions, with blue light inducing a greater myopic shift (M = −0.987 D) compared to red light (M = −0.867 D). This variation may be attributed to the Purkinje effect, where increased sensitivity to blue light during the transition from cone to rod vision tends to induce myopia (Koomen et al., 1951). This mechanism is consistent with our findings where the absolute value of M under blue light was higher than under red light. Other studies found that exposure to red light resulted in axial elongation, and blue light resulted in inhibition of axial elongation in human eyes (Thakur et al., 2021).

The literature reviewed presents three main theories regarding the causes of myopic shifts in low-light conditions: spherical aberration, chromatic aberration, and accommodation, yet consensus on the

primary cause remains elusive. Old studies such as those by Koomen et al. (KOOMEN et al., 1953) already highlighted that spherical aberration significantly contributed to myopization under low-light conditions, attributed to pupil dilation and subsequent increase in spherical aberration. In our study, despite maintaining a fixed pupil size of 4 mm across all conditions, significant differences in primary spherical aberration C(4.0) were observed between scotopic and mesopic, as well as between red light and blue light conditions. Moreover, secondary spherical aberration C(6.0) showed significant differences in scotopic conditions compared to other illuminations except baseline conditions. These findings suggest that while our study found subtle differences in M between mesopic, scotopic, and photopic conditions, larger pupil diameters might amplify these differences due to increased spherical aberration.

The difference in M between scotopic and mesopic compared to photopic is −0.106 D and −0.211 D respectively, in both cases less than −0.250 D. Regarding the blur polynomial C(2.0), the difference is also minimal (photopic 0.663 μm, mesopic 0.762 μm and scotopic 0.672 μm), so the results are not as high as in the studies mentioned above (Koomen et al., 1951). Apart from fixed pupil size, myopia may vary based on a study by Cabello et al. (Cabello, 1945), which found changes after 20 min of darkness, while this experiment used a 5-min adaptation period for each illumination.

The Zernike polynomial values obtained under mesopic, scotopic, and baseline conditions were highly similar, indicating a greater myopic tendency compared to photopic, blue light, and red light conditions. This observation correlates with findings on nocturnal myopia, where lower light levels are associated with increased myopic values (Koomen et al., 1951). Spherical aberration is identified as a significant factor influencing these results, particularly evident in comparisons involving primary and secondary spherical aberrations under scotopic conditions (excluding baseline lighting). The variation in M could potentially differ with varying pupil sizes other than the fixed 4 mm used in our study, as larger pupil sizes typically lead to greater spherical aberration. Lastly, chromatic aberration also plays a role, as shorter wavelengths, such as those in blue light compared to red light, induce greater myopic shifts in ocular behavior.

4.3. Retinal morphology-aberrations relationship

Our study found that retinal curvature and ocular aberrations were influenced by different lighting conditions, with the retina appearing flatter under scotopic and blue light conditions and more curved under mesopic conditions. These changes in retinal shape, along with increased spherical aberrations and defocus under lower light levels, suggest that dim and short-wavelength light may contribute to myopic shifts in vision due to optical defocus and aberration changes. This is consistent with earlier findings that dim lighting and blue light exposure can affect ocular optics and potentially influence myopia progression by altering retinal function and eye growth (Charman, 2005; Fernandez-Alonso et al., 2024; Norton and Siegwart, 2013). Research has proposed that blue light may trigger structural adaptations in the retina through increased signalling by ipRGCs, affecting eye growth regulation. Additionally, changes in retinal blood flow and metabolic demand under different lighting conditions may play a role in the eye's response to light (Antemie et al., 2023; Chistyakov et al., 2020; Penn et al., 2008). Understanding these mechanisms provides insight into how specific lighting conditions could influence retinal morphology and refractive changes, with potential implications for strategies to manage myopia progression.

In red light, the increased retinal curvature observed may result from its longer wavelength interacting differently with the eye's optics, affecting refractive state and retinal shape. The density and arrangement of red cones in the retina, along with changes in choroidal thickness, since the choroid modulates retinal shape in response to light exposure, could further contribute to this effect. Longer wavelengths penetrate deeper into ocular tissues and may influence these changes in retinal morphology (Lou and Ostrin, 2020; Zhao et al., 2023). This aligns with evidence that photoreceptor and choroidal responses work together in retinal adaptation to various light conditions (Cameron et al., 2020), suggesting a need for further research to confirm these dynamics.

Blue light exposure triggers myopic defocus through alterations in retinal signaling pathways via ipRGCs, contributing to myopia development (Cameron et al., 2020). Conversely, red light exposure affects photoreceptor activity and choroidal responses, potentially influencing refractive status differently (Chen et al., 2024; Zhang and Zhu, 2022). Therefore, exploring how various wavelengths modulate ocular growth and refractive changes offers new avenues for targeted interventions aimed at mitigating myopia progression.

5. Conclusion

In conclusion, the eye's adaptation to different lighting conditions affects both retinal curvature and ocular aberrations, with the greatest variations observed under mesopic and scotopic conditions. This highlights the significant influence of lighting on retinal morphology and the optical quality of the eye. Thus, the retina is flatter under scotopic and blue light conditions and more curved under mesopic conditions. Spherical aberrations and defocus increase with lower luminosity, suggesting that lighting affects retinal curvature and ocular refraction, influencing myopia.

CRediT authorship contribution statement

Elvira Orduna-Hospital: Writing – review & editing, Writing – original draft, Visualization, Validation, Supervision, Software, Resources, Project administration, Methodology, Investigation, Funding acquisition, Formal analysis, Conceptualization. **Juan J. Sanchez-Bautista:** Writing – original draft, Software, Methodology, Investigation, Formal analysis, Data curation. **Guisela Fernández-Espinosa:** Writing – original draft, Visualization, Validation, Software, Methodology, Investigation, Formal analysis, Data curation, Conceptualization. **María Arcas-Carbonell:** Writing – original draft, Visualization, Validation, Software, Methodology, Investigation, Formal analysis, Data curation, Conceptualization. **Ana Sanchez-Cano:** Writing – review & editing, Writing – original draft, Visualization, Validation, Supervision, Software, Resources, Project administration, Methodology, Investigation, Funding acquisition, Formal analysis, Conceptualization.

Declaration of generative AI and AI-assisted technologies in the writing process

During the preparation of this work the authors used ChatGPT to assist with drafting, editing, and refining the manuscript. After using this tool/service, the authors reviewed and edited the content as needed and take full responsibility for the content of the publication.

Funding

This research did not receive any specific grant from funding agencies in the public, commercial, or not-for-profit sectors.

Declaration of competing interest

The authors declare that they have no known competing financial interests or personal relationships that could have appeared to influence the work reported in this paper.

ABBREVIATIONS

AL	Axial length
CEICA	Clinical Research Ethics Committee of Aragón
e	Eccentricity
HOA	High order aberrations
ipRGCs	Intrinsically photosensitive ganglion cells
LOA	Low order aberrations
M	Spherical equivalent
MRI	Magnetic Resonance Imaging
OD	Right eye
OCT	Optical coherence tomography
PSF	Point spread function
Q	Asphericity
RPE	Retinal pigmented epithelium
SCN	Suprachiasmatic nucleus
SF	Shape factor
VA	Visual acuity

Data availability

Data will be made available on request.

References

Antemie, R.-G., Samoilă, O.C., Clichici, S.V., 2023. Blue light-ocular and systemic damaging effects: a narrative review. Int. J. Mol. Sci. 24. https://doi.org/10.3390/ijms24065998.

Artal, P., Schwarz, C., Cánovas, C., Mira-Agudelo, A., 2012. Night myopia studied with an adaptive optics visual analyzer. PLoS One 7, e40239.

Atchison, D.A., Jones, C.E., Schmid, K.L., Pritchard, N., Pope, J.M., Strugnell, W.E., Riley, R.A., 2004. Eye shape in emmetropia and myopia. Investig. Ophthalmol. Vis. Sci. 45, 3380–3386. https://doi.org/10.1167/iovs.04-0292.

Atchison, D.A., Pritchard, N., Schmid, K.L., Scott, D.H., Jones, C.E., Pope, J.M., 2005. Shape of the retinal surface in emmetropia and myopia. Investig. Ophthalmol. Vis. Sci. 46, 2698–2707. https://doi.org/10.1167/iovs.04-1506.

Atchison, D.A., Rozema, J.J., 2023. Technical notes on peripheral refraction, peripheral eye length and retinal shape determination. Ophthalmic Physiol. Opt. J. Br. Coll. Ophthalmic Opt. 43, 584–594. https://doi.org/10.1111/opo.13097.

Atchison, D.A., Smith, G., 2023. Optics of the human eye: second edition. Opt. Hum. Eye Second Ed 1–478. https://doi.org/10.1201/9781003128601/OPTICS-HUMAN-EYE-DAVID-ATCHISON.

Baumann, M., Gentile, R.C., Liebmann, J.M., Ritch, R., 1998. Reproducibility of retinal thickness measurements in normal eyes using optical coherence tomography. Ophthalmic Surg. Laser. 29, 280–285.

Beenakker, J.W.M., Shamonin, D.P., Webb, A.G., Luyten, G.P.M., Stoel, B.C., 2015. Automated retinal topographic maps measured with magnetic resonance imaging. Investig. Ophthalmol. Vis. Sci. 56, 1033–1039. https://doi.org/10.1167/iovs.14-15161.

Cabello, J., 1945. Causes of Night Myopia. An. la Soc. Española Física y Química, pp. 439–481.

Cameron, M.A., Morley, J.W., Pérez-Fernández, V., 2020. Seeing the light: different photoreceptor classes work together to drive adaptation in the mammalian retina. Curr. Opin. Physiol. 16, 43–49.

Charman, W.N., 2005. Aberrations and myopia. Ophthalmic Physiol. Opt. J. Br. Coll. Ophthalmic Opt. 25, 285–301. https://doi.org/10.1111/j.1475-1313.2005.00297.x.

Chen, Y.-Y., Tsai, T.-H., Liu, Y.-L., Lin, H.-J., Wang, I.-J., 2024. The impact of light properties on ocular growth and myopia development. Taiwan J. Ophthalmol. 14, 143–150. https://doi.org/10.4103/tjo.TJO-D-24-00031.

Cheng, H.M., Singh, O.S., Kwong, K.K., Xiong, J., Woods, B.T., Brady, T.J., 1992. Shape of the myopic eye as seen with high-resolution magnetic resonance imaging. Optom. Vis. Sci. 69, 698–701. https://doi.org/10.1097/00006324-199209000-00005.

Cheng, S.C.K., Lam, C.S.Y., Yap, M.K.H., 2010. Retinal thickness in myopic and non-myopic eyes. Ophthalmic Physiol. Opt. 30, 776–784.

Chin, N.B., Horn, R.E., 1956. Infrared skiascopic measurements of refractive changes in dim illumination and in darkness. JOSA 46 (1), 60–66. https://doi.org/10.1364/JOSA.46.000060, 46, 60–66.

Chistyakov, D.V., Baksheeva, V.E., Tiulina, V.V., Goriainov, S.V., Azbukina, N.V., Gancharova, O.S., Arifulin, E.A., Komarov, S.V., Chistyakov, V.V., Tikhomirova, N. K., Zamyatnin, A.A., Philippov, P.P., Senin, I.I., Sergeeva, M.G., Zernii, E.Y., 2020. Mechanisms and treatment of light-induced retinal degeneration-associated inflammation: insights from biochemical profiling of the aqueous humor. Int. J. Mol. Sci. 21. https://doi.org/10.3390/ijms21030704.

Faria-Ribeiro, M., López-Gil, N., Navarro, R., Lopes-Ferreira, D., Jorge, J., González-Méijome, J.M., 2014. Computing retinal contour from optical biometry. Optom. Vis. Sci. 91, 430–436. https://doi.org/10.1097/OPX.0000000000000225.

Fernandez-Alonso, M., Finch, A.P., Love, G.D., Read, J.C.A., 2024. Ocular accommodation and wavelength: the effect of longitudinal chromatic aberration on the stimulus-response curve. J. Vis. 24, 11. https://doi.org/10.1167/jov.24.2.11.

Frisken, S., Anderson, T., Segref, A., Lorenser, D., Frisken, G., 2023. Anterior and posterior imaging with hyperparallel OCT. Biomed. Opt Express 14, 2678. https://doi.org/10.1364/boe.488810.

Holladay, J.T., Janes, J.A., 2002. Topographic changes in corneal asphericity and effective optical zone after laser in situ keratomileusis. J. Cataract Refract. Surg. 28, 942–947. https://doi.org/10.1016/s0886-3350(02)01324-x.

Ishii, K., Iwata, H., Oshika, T., 2011. Quantitative evaluation of changes in eyeball shape in emmetropization and myopic changes based on elliptic Fourier descriptors. Investig. Ophthalmol. Vis. Sci. 52, 8585–8591. https://doi.org/10.1167/iovs.11-7221.

Kofuji, P., Mure, L.S., Massman, L.J., Purrier, N., Panda, S., Engeland, W.C., 2016. Intrinsically photosensitive retinal ganglion cells (ipRGCs) are necessary for light entrainment of peripheral clocks. PLoS One 11, e0168651.

Koomen, M., Scolnik, R., Tousey, R., 1953. Measurement of accommodation in dim light and in darkness by means of the Purkinje images. JOSA 43 (1), 27–31. https://doi.org/10.1364/JOSA.43.000027, 43, 27–31.

Koomen, M., Tousey, R., Scolnik, R., 1951. A study of night myopia. JOSA 41 (2), 80–90. https://doi.org/10.1364/JOSA.41.000080, 41, 80–90.

Koumbo Mekountchou, I.O., Conrad, F., Sankaridurg, P., Ehrmann, K., 2020. Peripheral eye length measurement techniques: a review. Clin. Exp. Optom. 103, 138–147. https://doi.org/10.1111/cxo.12892.

Li, Q., Fang, F., 2021. Retinal contour modelling to reproduce two-dimensional peripheral spherical equivalent refraction. Biomed. Opt Express 12, 3948. https://doi.org/10.1364/boe.426413.

Lim, L.S., Matsumura, S., Htoon, H.M., Tian, J., Lim, S. Bin, Sensaki, S., Chen, C., Hilal, S., Wong, T.Y., Cheng, C.Y., Kuo, A., Saw, S.M., 2020. MRI of posterior eye shape and its associations with myopia and ethnicity. Br. J. Ophthalmol. 104, 1239–1245. https://doi.org/10.1136/bjophthalmol-2019-315020.

Lindenmaier, A.A., Conroy, L., Farhat, G., DaCosta, R.S., Flueraru, C., Vitkin, I.A., 2013. Texture analysis of optical coherence tomography speckle for characterizing biological tissues in vivo. Opt. Lett. 38, 1280–1282. https://doi.org/10.1364/OL.38.001280.

Liu, B., Wang, Y., Li, T., Lin, Y., Ma, W., Chen, X., Lyu, C., Li, Y., Lu, L., 2018. Correlation of subfoveal choroidal thickness with axial length, refractive error, and age in adult highly myopic eyes. BMC Ophthalmol. 18, 1–5. https://doi.org/10.1186/s12886-018-0791-5.

Lou, L., Ostrin, L.A., 2020. Effects of narrowband light on choroidal thickness and the pupil. Investig. Ophthalmol. Vis. Sci. 61. https://doi.org/10.1167/IOVS.61.10.40.

McNabb, R.P., Polans, J., Keller, B., Jackson-Atogi, M., James, C.L., Vann, R.R., Izatt, J. A., Kuo, A.N., 2019. Wide-field whole eye OCT system with demonstration of quantitative retinal curvature estimation. Biomed. Opt Express 10, 338. https://doi.org/10.1364/boe.10.000338.

Mohd-Ali, B., Chen, L.Y., Shahimin, M.M., Arif, N., Hamid, H.A., Halim, W.H.W.A., Mokri, S.S., Huddin, A.B., Mohidin, N., 2022. Ocular dimensions by three-dimensional magnetic resonance imaging in emmetropic versus myopic school children. Med. Hypothesis, Discov. Innovation (MEHDI) Ophthalmol. 11, 64–70. https://doi.org/10.51329/mehdiophthal1447.

Monk, T.H., Weitzman, E.D., Fookson, J.E., Moline, M.L., Kronauer, R.E., Gander, P.H., 1983. Task variables determine which biological clock controls circadian rhythms in human performance. Nature 304, 543–545.

Norton, T.T., Siegwart, J.T.J., 2013. Light levels, refractive development, and myopia–a speculative review. Exp. Eye Res. 114, 48–57. https://doi.org/10.1016/j.exer.2013.05.004.

Orduna-Hospital, E., Crespo-Castan, C., Ávila, F.J., Sanchez-Cano, A., 2023. Adaptive illuminance effects on retinal morphology and refraction: a comprehensive study of night myopia. J. Clin. Med. 13, 211.

Penn, J.S., Madan, A., Caldwell, R.B., Bartoli, M., Caldwell, R.W., Hartnett, M.E., 2008. Vascular endothelial growth factor in eye disease. Prog. Retin. Eye Res. 27, 331–371. https://doi.org/10.1016/j.preteyeres.2008.05.001.

Pope, J.M., Verkicharla, P.K., Sepehrband, F., Suheimat, M., Schmid, K.L., Atchison, D. A., 2017. Three-dimensional MRI study of the relationship between eye dimensions, retinal shape and myopia. Biomed. Opt Express 8, 2386–2395. https://doi.org/10.1364/BOE.8.002386.

Sala-Puigdollers, A., Figueras-Roca, M., Hereu, M., Hernández, T., Morató, M., Adán, A., Zarranz-Ventura, J., 2018. Repeatability and reproducibility of retinal and choroidal thickness measurements in diabetic macular edema using swept-source optical coherence tomography. PLoS One 13, e0200819.

Sanchez-Cano, A., Orduna, E., Segura, F., Lopez, C., Cuenca, N., Abecia, E., Pinilla, I., 2014. Choroidal thickness and volume in healthy young white adults and the relationships between them and axial length, ammetropy and sex. Am. J. Ophthalmol. 158, 574–583.

Sergeeva, M., Borisova, O., Romanchuk, N., Videnin, A., Pyatin, V., Shusharina, N., Zakharov, A.V., Kolsanov, A., 2023. The effect of circadian photoreceptors stimulation on the stress response of subjects with high anxiety: a pilot study. Appl. Sci. 13, 6679.

Spaide, R.F., Curcio, C.A., 2011. Anatomical correlates to the bands seen in the outer retina by optical coherence tomography: literature review and model. Retina 31, 1609–1619.

Thakur, S., Dhakal, R., Verkicharla, P.K., 2021. Short-term exposure to blue light shows an inhibitory effect on axial elongation in human eyes independent of defocus. Investig. Ophthalmol. Vis. Sci. 62. https://doi.org/10.1167/iovs.62.15.22.

Van Dongen, H.P.A., Dinges, D.F., 2000. Circadian rhythms in fatigue, alertness, and performance. Princ. Pract. sleep Med. 20, 391–399.

Verkicharla, P.K., Mathur, A., Mallen, E.A.H., Pope, J.M., Atchison, D.A., 2012. Eye shape and retinal shape, and their relation to peripheral refraction. Ophthalmic Physiol. Opt. 32, 184–199. https://doi.org/10.1111/j.1475-1313.2012.00906.x.

Verkicharla, P.K., Suheimat, M., Schmid, K.L., Atchison, D.A., 2017. Differences in retinal shape between east asian and caucasian eyes. Ophthalmic Physiol. Opt. 37, 275–283. https://doi.org/10.1111/opo.12359.

Verkicharla, P.K., Suheimat, M., Schmid, K.L., Atchison, D.A., 2016. Peripheral refraction, peripheral eye length, and retinal shape in Myopia. Optom. Vis. Sci. 93, 1072–1078. https://doi.org/10.1097/OPX.0000000000000905.

Wald, G., Griffin, D.R., 1947. The change in refractive power of the human eye in dim and bright light. JOSA 37 (5), 321–336. https://doi.org/10.1364/JOSA.37.000321, 321-336 37.

Wirz-Justice, A., Skene, D.J., Münch, M., 2021. The relevance of daylight for humans. Biochem. Pharmacol. 191, 114304. https://doi.org/10.1016/j.bcp.2020.114304.

Zhang, P., Zhu, H., 2022. Light signaling and myopia development: a review. Ophthalmol. Ther 11, 939–957.

Zhao, C., Ni, Y., Zeng, J., 2023. Effect of red-light therapy on retinal and choroidal blood perfusion in myopic children. Ophthalmic Physiol. Opt. J. Br. Coll. Ophthalmic Opt. 43, 1427–1437. https://doi.org/10.1111/opo.13202.

Zhu, H., Liu, C., Gao, M., Zhang, S., Zhang, L., Zhao, Q., 2023. Choroidal thickness in relation to diopter and axial length among myopic children. Front. Med. 10, 1–9. https://doi.org/10.3389/fmed.2023.1241352.